

Accepted for publication in the Astrophysical Journal

# Chandra X-ray Imaging and Spectroscopy of the M87 Jet and Nucleus

A. S. Wilson<sup>1</sup> and Y. Yang

*Astronomy Department, University of Maryland, College Park, MD 20742;  
wilson@astro.umd.edu, yyang@astro.umd.edu*

## ABSTRACT

We report X-ray imaging - spectroscopy of the jet of M87 at sub arc second resolution with the Chandra X-ray Observatory. The galaxy nucleus and all the knots seen at radio and optical wavelengths, as far from the nucleus as knot C, are detected in the X-ray observations. There is a strong trend for the ratio of X-ray to radio, or optical, flux to decline with increasing distance from the nucleus. At least three knots are displaced from their radio/optical counterparts, being tens of pc closer to the nucleus at X-ray than at radio or optical wavelengths. The X-ray spectra of the nucleus and knots are well described by power laws absorbed by cold gas, with only the unresolved nucleus exhibiting intrinsic absorption. In view of the similar spectra of the nucleus and jet knots, and the high X-ray flux of the knots closest to the nucleus, we suggest that the X-ray emission coincident with the nucleus may actually originate from the pc – or sub-pc – scale jet rather than the accretion disk.

Arguments are given that the X-ray emission process is unlikely to be inverse Compton scattering. Instead, we favor synchrotron radiation. Plotted as  $\nu S_\nu$ , the spectra of the knots generally peak in or just above the optical - near infrared band. However, the overall spectra of at least three knots cannot be described by simple models in which the spectral index monotonically increases with frequency, as would result from synchrotron losses or a high energy cut-off to the injected electron spectrum. Instead, these spectra must turn down just above the optical band and then flatten in the X-ray band. In the context of a synchrotron model, this result suggests that either the X-ray emitting electrons/positrons in

---

<sup>1</sup>Adjunct Astronomer, Space Telescope Science Institute, 3700 San Martin Drive, Baltimore, MD 21218; awilson@stsci.edu

these knots represent a separate “population” from those that emit the radio and optical radiation or the magnetic field is highly inhomogeneous. If the former interpretation is correct, our results provide further support for the notion that radio galaxies produce a hard ( $\gamma \simeq 2 - 2.5$ ,  $N(E) \propto E^{-\gamma}$ ) spectrum of high energy ( $E/m_e c^2 \sim 10^{7-8}$ ) electrons and possibly positrons.

*Subject headings:* galaxies: active – galaxies: individual (M87) – galaxies: jets – galaxies: nuclei – magnetic fields – X-rays: galaxies

## 1. INTRODUCTION

The jet in M87 is arguably the most famous of its kind, primarily because of its proximity and strong optical synchrotron radiation. It has been studied in great detail at radio (see Biretta 1999 for a review) and optical (e.g. Biretta, Sparks & Macchetto 1999; Perlman et al. 2001) wavelengths. Radio observations of the jet show that it is polar down to 0.01 pc (Junor & Biretta 1995), which is only 60 times the gravitational radius of the black hole (mass  $\simeq 3 \times 10^9 M_\odot$ , e.g. Macchetto et al. 1997). HST observations have revealed numerous features in the inner  $\simeq 400$  pc with speeds in the range  $4c$  to  $6c$ , confirming that the bulk flow of the jet is relativistic (Biretta, Sparks & Macchetto 1999).

At X-ray wavelengths, the nucleus and knot A have been detected (Schreier, Gorenstein & Feigelson 1982; Biretta, Stern & Harris 1991; Neumann et al. 1997; Harris, Biretta & Junor 1997; Böhringer et al. 2001). The limited resolution of prior X-ray telescopes has precluded a study with comparable resolution to optical telescopes. With the advent of the Chandra X-ray Observatory, it is now possible to obtain imaging - spectroscopy of the jet with sub arc second resolution.

In Section 2, we describe the Chandra observations and the data reduction. Section 3 presents the results, discussing the morphology of the jet and the spectra of the nucleus and individual jet knots. Section 4 is devoted to the radiation mechanism of the X-rays, while Section 5 summarises our conclusions. We assume a distance of 16 Mpc (Tonry 1991; Whitmore et al. 1995), so  $1'' = 78$  pc. The Galactic column density in the direction of M87 is  $N_H(\text{Gal}) = 2.5 \times 10^{20} \text{ cm}^{-2}$  (Stark et al. 1992).

## 2. OBSERVATIONS AND DATA REDUCTION

Because the nucleus and knot A of the jet are known to be strong X-ray emitters, we were concerned that use of the default 3.2s frame time for ACIS would result in pile-up in these and possibly other regions. We therefore obtained a short ( $< 1$  ks) exploratory observation of M87 on April 20 2000 (obsid 351) with the nucleus at the aim point on ACIS-S (chip S3). This observation was made in so called “alternating mode”, with the frame time alternating between 0.1 and 0.4s. This observation showed the peak, level 2 count rate to be  $\simeq 0.10$  cts  $\text{s}^{-1}$  pixel $^{-1}$  for both frame times, implying that observations with a 3.2s frame time would suffer significantly from pile-up, but that observations with a 0.4s frame time would be free of it.

The science observations were, therefore, taken in two parts. First, an observation with a 3.2s frame time was obtained on July 29 2000 (obsid 352). CCDs I2, I3, S1, S2, S3 and S4 were on and the good exposure time (LIVTIME) was 37.6 ks. This observation was designed for study of the cluster and the fainter parts of the jet. Second, an observation with 0.4s frame time was taken on July 30 2000 (obsid 1808). Only S3 was used, and the exposed region comprised a band 127 rows (62'') wide with length the whole chip. The width of the band suffices to include the whole jet. The good exposure time was 12.8 ks. The peak count rate at the nucleus in this exposure is  $0.07$  cts  $\text{s}^{-1}$  pixel $^{-1}$ , which is different to that obtained in the exploratory exposure, suggesting variability of the nucleus between April 20 and July 30 2000 (the corresponding total count rates from the nucleus are  $0.55$  and  $0.39$  cts  $\text{s}^{-1}$  for these two dates, respectively). This count rate confirms that the nucleus is not piled-up in a 0.4s frame time. From this second exposure, we have obtained spectra of the brighter regions in the field, specifically the nucleus and the brighter parts of the jet.

We followed the procedures recommended in the “science threads”, including filtering of data for times of high background and aspect errors, of which there were very few, and construction of response matrix functions and ancillary response files at the locations of the nucleus and knots of the jet. In order to improve the sampling of the image, we interpolated to a pixel size of  $0''.1$  and then smoothed the data with a Gaussian of  $\text{FWHM} = 0''.5$ . Processing of the data initially used ciao 1.1.5, but on March 19 2001 reprocessed data were received, which must be processed with ciao 2. We made a careful comparison of the results of processing the old data with ciao 1.1.5 and the new data with ciao 2 and found no significant differences.

While this paper was being written (July 2001), preliminary versions of new response functions (“fefs”) became available. We reprocessed the spectra of knot A with these new functions and found that all parameters of the absorbed power law model spectra ( $N_{\text{H}}$ ,  $\Gamma$  and  $K$ , see Table 2) were within the 90% confidence error ranges of the parameters obtained with

the old response functions. For uniformity, we give only parameters obtained with the old response functions, which are quite adequate for dealing with continuum spectra, as found in the M87 jet.

### 3. RESULTS

#### 3.1. Astrometry and Morphology

A grey scale image and a contour map of the jet (from the 3.2s frame time observation) are shown in Fig. 1, while Fig. 2 compares radio, optical and X-ray images with similar FWHM resolutions -  $0''.4$ ,  $0''.7$  and  $\simeq 0''.7$ , respectively. The position of the X-ray nucleus (in J2000.0 coordinates) is  $RA_x = 12^h 30^m 49^s.40$ ,  $Dec_x = 12^\circ 23' 27''.8$ . This may be compared with two VLA radio positions -  $RA_{r1} = 12^h 30^m 49^s.423$ ,  $Dec_{r1} = 12^\circ 23' 28''.11$  from an archival 15 GHz map made by Carole Mundell and  $RA_{r2} = 12^h 30^m 49^s.423$ ,  $Dec_{r2} = 12^\circ 23' 28''.02$  from a 5 GHz map provided by John Biretta. The differences are  $RA_x - RA_{r1} = -0''.3$ ,  $Dec_x - Dec_{r1} = -0''.3$ , and  $RA_x - RA_{r2} = -0''.3$ ,  $Dec_x - Dec_{r2} = -0''.2$ , which represent excellent agreement. No attempt has been made to remove the X-ray emission associated with knot HST-1, which has probably “pulled” the nuclear peak slightly westward; correction for this effect may improve the agreement in right ascension.

A casual examination of Fig. 2 shows the X-ray image to be similar to those in the other wavebands, with the nucleus, and jet knots HST-1, D, E, F, I, A, B and C (listed in order of increasing distance from the nucleus) all visible (we follow the traditional nomenclature, see e.g. Perlman et al. 2001). However, it is clear that the knots closest to the nucleus - HST-1 and D - are much brighter relative to the other knots than at radio and optical wavelengths. We discuss the spectral differences between the knots quantitatively in Section 3.2.

The centroid position of each knot has been measured using the iraf task ‘center’. We have also determined the position of the peak of emission through interpolation using the  $3 \times 3$  pixels centered on the brightest one. These two positions do not always agree because of internal structure and asymmetries in the brightness distributions of individual knots. Table 1 lists the distance of each knot from the nucleus in each waveband. When two numbers are listed separated by a dash, they represent the distances of the centroid and the peak from the nucleus, giving an approximate idea of the range resulting from internal structure. It is clear from Table 1 and the intensity profiles along the jet plotted in Fig. 3 that the X-ray emission of knots D and F is closer to the nucleus than at radio and optical wavelengths at these spatial resolutions. The X-ray emission of knots E and B may also be closer to the nucleus than their radio and optical counterparts, but here the effect is marginal. Comparison with the

much higher resolution HST optical observations (Perlman et al. 2001) shows that the X-ray emission of knot D peaks close to the optical emission of sub-knot D-East, while the X-ray emission of knot F is located near the upstream edge of the optical knot. Measurement of the position of knot A is complicated by the asymmetric structure found in higher resolution ( $0''.1 - 0''.2$ ) maps than shown here at both radio (e.g. Owen, Hardee & Cornwell 1989) and optical (Perlman et al. 2001) wavelengths. However, the present observations show that the distance from the nucleus to knot A is the same at all three wavelengths to within  $\pm 0''.1$ . This conclusion differs from that of Neumann et al. (1997) who found, based on ROSAT observations, that the X-ray maximum of knot A is situated  $0''.4$  nearer to the nucleus than the radio maximum. Neumann et al.’s (1997) finding undoubtedly results from the inclusion of the X-ray bright knots HST-1 and D in their nuclear source given the  $5''$  resolution of the ROSAT HRI. If the Chandra image is smoothed to this resolution, the separation of the “nuclear” and knot A peaks becomes  $11''.6$ , in reasonable agreement with Neumann et al.’s (1997) result.

Fig. 3 shows profiles of the radio, optical and X-ray brightnesses along the jet. The brightnesses have been normalised to be the same at knot A. In this representation, the X-ray emission lies above the radio and optical closer to the nucleus than knots A and F (i.e. for knots HST-1, D and E) but below the radio and optical beyond knot A (i.e. for knots B and C). The X-ray emission of the jet thus declines more rapidly with increasing distance from the nucleus than does the radio or optical emission.

### 3.2. Spectra

X-ray spectra have been obtained for the nucleus and all knots out to knot C. Background spectra were taken for each knot from two regions just outside the jet and along a line perpendicular to it passing through the knot in question. The spectra obtained are insensitive to the exact choice of background since the jet is very bright compared to its surroundings. The spectra of all knots were modelled with a power law absorbed by cold matter. The resulting equivalent hydrogen column density, photon index and normalisation of the spectra are given in Table 2. Our photon indices for the nucleus and knot A are in excellent agreement with those obtained by XMM (Böhringer et al. 2001), though the latter data average over a larger area. Knot HST-1 is significantly contaminated by nuclear emission so we do not list the parameters of its spectrum. However, its spectrum appears to be well described by a power law with index  $\Gamma = 2.24$ , similar to the rest of the jet. Deconvolution (deferred to a later paper) will be necessary to obtain a more reliable measure of its spectral parameters.

Of the jet knots, only knot F shows evidence of an absorbing column in excess of the Galactic column of  $N_{\text{H}}(\text{Gal}) = 2.5 \times 10^{20} \text{ cm}^{-2}$ . This possible excess should be treated with caution in view of uncertainties in the instrumental response below 0.4 keV. On the other hand, the nucleus shows clear excess absorption of  $\simeq (3 - 5) \times 10^{20} \text{ cm}^{-2}$  over the Galactic column (Table 2). Comparison of the model absorbed and unabsorbed spectra shows that this absorption is too large to be an instrumental error.

The photon indices of the nucleus and all knots are quite similar (Table 2), ranging between best estimate values of  $\Gamma = 2.04$  and 2.90 (flux spectral indices  $\alpha$  between 1.04 and 1.90). The similarity of the nuclear spectrum to that of the jet and the strong increase of the brightness of the X-ray jet towards the nucleus (Fig. 3) suggests that the “nuclear” emission may actually originate from the pc – or sub-pc – scale jet. Various VLBI observations have imaged the jet down to milli arc second scales (e.g. Junor & Biretta 1995), and it is reasonable that there should be X-ray emission from the jet unresolved by Chandra.

Fig. 4 shows radio through X-ray spectra for eight knots plus the nucleus. Plotted as  $\nu S_\nu$ , the spectra are seen to turn over in or near the optical band, a phenomenon sometimes attributed to synchrotron losses (e.g. Perlman et al. 2001 and references therein). These broad band spectra are discussed later in the context of the X-ray emission process (Section 4).

Fig. 5 is a plot of the optical to X-ray ( $\alpha_{\text{ox}}$ ), radio to X-ray ( $\alpha_{\text{rx}}$ ) and X-ray ( $\alpha_{\text{x}}$ ) spectral indices of the knots as a function of distance from the nucleus. As can be seen, both  $\alpha_{\text{ox}}$  and  $\alpha_{\text{rx}}$  increase systematically with distance from the nucleus (the errors in these spectral indices are smaller than the symbol sizes). This is another way of saying that the X-ray emission declines more rapidly with increasing distance from the nucleus than does the radio or optical emission (Section 3.1 and Fig. 3).

## 4. The Nature of the X-ray Emission

### 4.1. Inverse Compton Scattering

A plausible process for X-ray emission from radio jets is inverse Compton scattering. The photons being upscattered can either be the synchrotron radiation (synchrotron self-Compton [SSC] process) or some external source (external Compton [EC]), such as the galaxy starlight, radiation from the active nucleus or the microwave background. The possibility of bulk relativistic motion by the jet needs to be considered (see e.g. Begelman, Blandford & Rees 1984 for a review). We consider the cases with and without relativistic motion in the next two subsections.

#### 4.1.1. No bulk relativistic motion

We have performed numerical calculations of spectra in spherical geometries using the computer code of Band & Grindlay (1985, 1986), which was kindly provided by D. E. Harris. Equipartition fields for the knots are given by Owen, Hardee & Cornwell (1989) and are in the range  $(1.6 - 5.1) \times 10^{-4}$  gauss. We have calculated inverse Compton models for knot B, which should be representative of the other knots. Assuming the radio to optical spectrum given in Fig. 4 and low and high frequency cut-offs to the synchrotron radiation at  $10^7$  and  $10^{15}$  Hz (see Fig. 4 and Meisenheimer et al. 1996), we find the internal radiation density from synchrotron radiation to be  $\simeq 8 \times 10^{-10}$  erg cm $^{-3}$ , which exceeds other known sources of radiation (an exception might be a narrow beam of radiation from the nucleus and aligned with the jet, but we ignore this possibility here). The radiation density of the synchrotron radiation is, however, an order of magnitude below that of the equipartition magnetic field ( $B_{\text{eq}} \simeq 3 \times 10^{-4}$ ) plus relativistic particles, indicating the electrons/positrons lose energy mostly to synchrotron radiation. The calculation shows that the SSC radiation is  $\simeq 600$  times smaller than observed at 1 keV for an equipartition field. The emissivity  $\epsilon_{\nu}^{\text{SSC}} \propto N_{\text{e}0} \propto B^{-(\gamma+1)/2}$  (where  $\gamma$  is the exponent in the electron energy spectrum  $N(E) = N_{\text{e}0}E^{-\gamma}$ ) for a given synchrotron emissivity. Thus the field strength would have to be a factor  $\simeq 70$  times weaker than equipartition (given that  $\alpha = 0.48$  ( $S_{\nu} \propto \nu^{-\alpha}$ ) for knot B) for  $\epsilon_{\nu}^{\text{SSC}}$  to agree with the emissivity observed at 1 keV.

For inverse Compton scattering off the microwave background, the predicted intensity at 1 keV is  $10^{5-6}$  lower than observed for an equipartition field. These results render inverse Compton models extremely unlikely in the absence of bulk relativistic motion.

#### 4.1.2. Bulk relativistic motion

The above considerations must be modified if the material comprising the jet knots is moving relativistically. There is now clear evidence for such relativistic motions in the first 6'' of the jet based on HST observations of apparent speeds of features in the range  $4c - 6c$  (Biretta, Sparks & Macchetto 1999).

As usual, we use the Doppler factor  $\delta$  (where  $\delta = [L(1 - \beta \cos \theta)]^{-1}$ ,  $L$  is the Lorentz factor of the bulk flow,  $\beta$  is the bulk velocity in units of the speed of light, and  $\theta$  is the angle between the velocity vector and the line of sight). The expression for the ratio of SSC X-ray spectral flux to synchrotron radio spectral flux is often written in terms of parameters defining the synchrotron self absorption (SSA) turnover, such as  $\nu_{\text{m}}$  (frequency of SSA turnover) and  $S_{\text{m}}$  (flux density at  $\nu_{\text{m}}$ , extrapolated from the optically thin spectrum). In this case,  $S_{\nu, \text{SSC}}$

$\propto \delta^{-2(\alpha+2)}$  (Burbidge, Jones & O’Dell 1974; Marscher 1983). This parameterisation results from the historical tendency for the SSC model to be applied to compact radio sources with detected X-ray emission, for which  $\nu_m$  and  $S_m$  are directly measured (e.g. Marscher et al. 1979). However, in the case of extended jets and hot spots, SSA almost always occurs at too low a frequency to be observed, and it is more intuitive to express  $S_{\nu,SSC}$  in terms of  $N_{e0}$  and  $B$ . In this case, the dependence of SSC flux density on  $\delta$  for isotropic radiation in the blob’s rest frame is  $S_{\nu,SSC} \propto \delta^{3+\alpha}$ . This behavior is identical to the dependence for synchrotron radiation (also assumed isotropic in the blob’s rest frame),  $S_{\nu,synch} \propto \delta^{3+\alpha}$ , so the ratio  $S_{\nu,SSC}/S_{\nu,synch} \propto N_{e0}$  and is independent of  $\delta$  (Dermer, Sturmer & Schlickeiser 1997). We thus see that  $S_{\nu,SSC}/S_{\nu,synch}$  is unaffected by bulk relativistic motion given the assumption that the radiation is isotropic in the blob’s rest frame, and that the only way to increase the SSC flux density for a given radio flux density is to increase  $N_{e0}$  (or, equivalently, to decrease  $B$  [Sect 4.1.1]).

The situation is different for inverse Compton scattering of the microwave background. Here the radiation is isotropic in the comoving Hubble frame and anisotropic in the frame of the blob. Now the principal dependence of the external Compton scattered flux density is  $S_{\nu,EC} \propto \delta^{4+2\alpha}$  (Dermer 1995; Dermer, Sturmer & Schlickeiser 1997). Thus  $S_{\nu,EC}/S_{\nu,synch} \propto \delta^{1+\alpha}$  so the EC X-ray flux is boosted relative to the synchrotron radio flux if  $\delta > 1$ . In Section 4.1.1, we found that inverse Compton scattering off the microwave background fails by a factor of  $10^{5-6}$  to reproduce the observed X-ray flux density. Setting  $\delta^{1+\alpha} = 10^{5-6}$ , we find  $\delta \sim 10^4$  is required (for an equipartition field). Since, for a given angle  $\theta$ , the maximum value of  $\delta = \delta_{max} = 1/\sin \theta$ , the M87 jet would have to be aligned within  $\sim 1'$  of our line of sight, an implausibly small angle. In general, inverse Compton scattering by relativistic jets of the microwave background will produce a large boost in observed flux density only if the jet is aligned close to the line of sight.

Thus we conclude that inverse Compton models fail unless the magnetic field is weaker than equipartition by a large factor. In addition, inverse Compton radiation should have the same spectral index as power-law synchrotron radiation (away from the “end points”). However, Table 2 and Fig. 4 show that the X-ray spectrum is always steeper than the radio spectrum. A way out of this problem is to postulate the existence of a steep spectrum, low energy population of relativistic electrons. These electrons would radiate synchrotron radiation at lower frequencies than those at which the jet has been observed and would inverse Compton scatter photons to X-ray energies. Such models are *ad hoc* and also require that the low energy electron population is in an extremely weak magnetic field (see e.g. model 3, Table 4 and Fig. 9 of Wilson, Young & Shopbell [2001], which attempts to explain the properties of the western hot spot of Pictor A in terms of such a model). While it is impossible to rule out such models absolutely (the relevant relativistic electrons could be in



a region of weak or no magnetic field and thus radiate little or no synchrotron radiation), we consider all inverse Compton scattering models for the X-ray emission of the M87 jet to be extremely implausible.

## 4.2. Synchrotron Radiation

The X-ray emission of the jet is almost certainly synchrotron radiation, as preferred by several earlier workers (e.g. Biretta et al. 1991; Neumann et al. 1997). This hypothesis is favored by the steep X-ray spectra of the knots (Fig. 4), which presumably result, at least in part, from synchrotron losses given that the electrons have  $E/m_e c^2 \sim 10^{7-8}$  and half lives of order years. The optical spectra are also steeper than the radio, a result which has also been ascribed to synchrotron losses (e.g. Perlman et al. 2001). Our finding that both  $\alpha_{\text{ox}}$  and  $\alpha_{\text{rx}}$  increase systematically with increasing distance from the nucleus suggests a trend of either increasing synchrotron losses or decreasing high energy particle acceleration at larger nuclear distances. The latter effect might be related to deceleration of the jet.

Perlman et al. (2001) have shown that simple models involving synchrotron losses can match the optical spectra of individual knots. They considered a variety of possible situations and were able to exclude a model for knot A in which the electrons are continuously injected (CI) with the index of the electron energy spectrum being the same over the whole range of radio to X-ray emitting energies. In the CI model, both low and high frequency regimes are power laws with a difference in spectral index  $\Delta\alpha = 0.5$  (Ginzburg 1957; Kardashev 1962). Such a model that correctly accounts for the radio – optical spectrum of knot A overpredicts its X-ray flux. Perlman et al. (2001) showed that other models (e.g. Kardashev 1962; Jaffe & Perola 1973), in which there is no continuous injection of relativistic electrons at high energies, are able to account for the radio – optical spectra of several knots, with reasonable concurrence with the X-ray flux point then known for knot A. These authors also suggested that the weak X-ray flux might result if, for some reason, the corresponding relativistic electrons fill volumes much smaller than the optical emitting regions.

In general, the effect of a high energy cut-off or synchrotron/inverse Compton losses on the relativistic electron energy spectrum in a magnetic field of uniform strength is a synchrotron spectrum exhibiting a monotonically increasing slope (spectral index) with increasing frequency. Examination of the multi-band spectra (Fig. 4) shows that the radio through X-ray spectra of some knots (e.g. E, F, I) may be qualitatively consistent with this expectation. However, in other cases (knots A, B and probably D), the X-ray spectrum cannot be reproduced by extending the radio through optical fluxes with a spectrum having a monotonically increasing spectral index with increasing energy. In these cases, the spectrum

must turn down above the optical, and then flatten out to match the X-ray spectrum. This situation is identical to that found for the western hot spot of Pictor A (Fig. 8 of Wilson, Young & Shopbell 2001).

There are three general ways in which such spectra may arise, as we now discuss:

- (i) If the magnetic field does not depart greatly from uniform strength within any given knot, the X-rays must come from a different “population” of relativistic electrons from those responsible for the radio and optical emissions. In this case, the spectra turn down sharply above the optical band due to synchrotron losses or a high energy cutoff in the injection spectrum, with a separate “population” dominating the X-ray emission.
- (ii) The magnetic field departs greatly from uniformity.
- (iii) The X-ray and/or optical emission is highly variable, so that the X-rays have declined or the optical increased between the dates the optical (Feb or April 1998 for Perlman et al.’s [2001] HST data, the triangles in Fig. 4) and X-ray (July 30 2000) observations were made.

We discuss these three possibilities in turn.

In possibility (i), the index of the electron spectrum at injection  $\gamma_x = 2\alpha_x$  for the X-ray-emitting electrons/positrons (assuming an equilibrium between injection and synchrotron losses). Thus  $\gamma_x$  ranges between 2.08 and 3.80. The latter value of  $\gamma_x$  (for knot F) has large errors and most values of  $\gamma_x$  are  $\simeq 2.5 - 2.6$  (Table 2). These numbers are reasonably consistent with the latest expectations from diffusive shock acceleration theory, which gives  $\gamma \simeq 2.2$  (Kirk 2001). As well as being directly accelerated by shocks, high energy relativistic electrons may result from a “proton-induced cascade” initiated by photopion production; this process gives a synchrotron X-ray spectrum which is distinct from extrapolations of the synchrotron radio - optical spectrum (e.g. Mannheim, Krüls & Biermann 1991). The notion that the X-ray emission results from a separate, high energy component of relativistic electrons/positrons is consistent with the different morphologies and locations of some X-ray knots compared to the corresponding radio and optical knots (Section 3.1). In an earlier paper (Wilson, Young & Shopbell 2001), we noted, based on a very small sample, that *hot spots* which are overluminous in X-rays compared with the predictions of SSC models appear to be in environments with low intergalactic gas density. One speculative interpretation is that the resulting high outward velocity of the hot spots is conducive to acceleration of the  $E/m_e c^2 \sim 10^{7-8}$  particles needed for X-ray synchrotron emission. Such a scenario could also apply to the *jet* of M87 since superluminal proper motions have been detected out to  $6''$  from the nucleus, strongly suggesting the bulk motions of the jet are relativistic (Biretta et al. 1999).

Turning to possibility (ii), there is some literature on the properties of synchrotron radiation in inhomogeneous magnetic fields (e.g. Cavallo, Horstman & Muracchini 1980). An extreme proposal is Burn’s (1973) model of the Crab Nebula. Burn proposed that there is a large scale field, superimposed on which are regions of higher magnetic field strength, perhaps filamentary in morphology (the “wisps” would be examples) and produced by hydromagnetic disturbances, the energy source for which is the pulsar. The model does not require the usually-supposed continuous injection of high energy relativistic electrons. Instead, the radiation at frequencies higher than optical originates from electrons that are temporarily caught in regions of enhanced magnetic field, but which spend most of their time in lower fields when they radiate at radio and optical frequencies. Only a small fraction of the nebula has these high field regions, which must have strengths more than 100 times the undisturbed field in order to account for the extended X-ray emission of the nebula. The spectrum of the high frequency emission then reflects the spectrum of the magnetic field strength rather than that of the relativistic electrons. Since the magnetic field strength in the Crab and the M87 knots are similar (several  $\times 10^{-4}$  gauss), the qualitative character of the model would be similar in M87, with the hydromagnetic compressions being driven by the jet. In particular, the observed flat X-ray spectra of knots A, B and D would be related to the spectrum of the magnetic field strength. State-of-the-art, three dimensional MHD simulations of radio galaxies (e.g. Tregillis, Jones & Ryu 2001) can, in principle, address the crucial question of whether the very large enhancements of magnetic field strength required in Burn’s model are likely to occur in nature.

For possibility (iii) to apply, large flux variations are needed. For example, if the X-ray emission of knot B is to fall on a direct extension of the radio - optical spectrum with a monotonically increasing spectral index with increasing frequency, its flux would have to be at least 5 times larger than observed, assuming no change in  $\alpha_x$  (Fig. 4). Harris, Biretta & Junor (1997, 1999) have found a secular decrease (significant at the  $3\sigma$  level) in the intensity of knot A of some 16% between 1992 and 1997 based on ROSAT observations. Such small changes in X-ray flux are totally insufficient to resolve the discrepancy between the X-ray spectra of knots A, B and D and the extrapolations of their radio - optical spectra. Further, the four separate determinations of the optical spectra of knots D, A and B (Fig. 4) agree well, despite being taken over a period of 15 years (the observations of Biretta et al. [1991], Keel [1988], Pérez-Fournon et al. [1988] and Perlman et al. [2001] were taken in 1983, 1985, 1986 and 1998, respectively). Thus the present data suggest that variations as large as needed do not occur. However, given the limited angular resolution of the ROSAT observations, monitoring with Chandra is highly desirable and should be able to resolve the issue, especially if simultaneous optical spectra are obtained.

## 5. Conclusions

We have obtained high sensitivity, X-ray imaging - spectroscopy of the jet of M87 with sub arc second angular resolution. Superficially, the X-ray jet resembles that in the radio and optical bands, with all knots out to knot C detected. However, there is a very strong trend for the ratio of X-ray to either radio or optical flux to decline with increasing distance from the nucleus. This strength of the near-nuclear jet in X-rays suggests that the X-ray emission coincident with the nucleus may actually originate from the pc – or sub-pc – scale jet, rather than the accretion disk. There are clear morphological differences between the radio/optical jet, on the one hand, and the X-ray jet, on the other. In particular, some knots in the X-ray image are displaced from their radio/optical counterparts towards the nucleus by tens of pc.

The spectra of the nucleus and all jet knots may be well described by power-law spectra absorbed by cold matter. Only the nucleus shows clear evidence for intrinsic absorption, with an equivalent hydrogen column density of  $\sim (3 - 5) \times 10^{20} \text{ cm}^{-2}$ . The knots in the jet have photon indices,  $\Gamma$ , in the range 2.04 to 2.90, with average  $\Gamma \simeq 2.4$ . The X-ray spectra of the jet knots are thus considerably steeper than those at radio or optical wavelengths. Plotted as  $\nu S_\nu$ , the spectra of the knots peak in or somewhat above the optical - near infrared band.

We have discussed the process responsible for the X-ray emission. Synchrotron self-Compton emission falls short by a factor of  $\sim 100 - 1,000$  for an equipartition field. The field needs to be  $\sim 70$  times below equipartition to match the X-ray flux, independent of the Doppler factor  $\delta$ . Models invoking inverse Compton scattering of the microwave background require very large values of  $\delta$  and that the jet is closely aligned with our line of sight. Further, the spectral indices of the X-ray and radio emissions are very different, in contrast with the similar spectral indices expected if the synchrotron-emitting and inverse Compton scattering electron populations are the same. For these reasons, we consider all inverse Compton models to be extremely implausible.

The X-ray emission from the jet is almost certainly synchrotron radiation. However, for at least three knots, the X-ray spectrum is not a simple continuation of the radio – optical spectrum. Instead, the spectrum must turn down at frequencies above the optical – near infrared band, and then flatten in X-rays. The broad-band spectra of these knots is remarkably similar to that of the western hot spot of Pictor A. The optical, near infrared and X-ray data were not taken simultaneously, raising the possibility that our broad-band spectra may be affected by variability. However, the magnitude of the knot variability required to reconcile the observed spectra with simple synchrotron models, in which the spectral index increases monotonically with increasing frequency, is much larger than any yet observed. We briefly discuss the potential application to M87 of a model, originally due to Burn (1973),

in which the magnetic field is extremely inhomogeneous. In this model, the X-ray emission originates from low energy electrons temporarily in regions of very strong magnetic field; the X-ray spectrum is related to the spectrum of the strength of the magnetic field rather than the energy spectrum of the relativistic electrons. A third alternative is that the X-ray synchrotron-emitting electrons/positrons are a separate “population” (i.e. they have a different energy spectral index at injection), to those which emit the radio and optical synchrotron radiation. If the last alternative is correct, our X-ray spectra of the M87 jet provide additional support for the notion that radio galaxies produce a hard ( $\gamma = 2 - 2.5$ ) spectrum of high energy ( $E/m_e c^2 \sim 10^{7-8}$ ) electrons and possibly positrons.

We are grateful to John Biretta and Ismael Pérez-Fournon for providing a 6 cm VLA map and a V band image of the jet, respectively, and to Carole Mundell for making a 2 cm map from the VLA archive. We thank the staff of the Chandra Science Center, especially D. E. Harris and S. Virani, for their help, C. D. Dermer for a valuable correspondence and E. S. Perlman for helpful comments. This research was supported by NASA through grants NAG 81027 and NAG 81755.

## REFERENCES

- Band, D. L. & Grindlay, J. E. 1985, *ApJ*, 298, 128
- Band, D. L. & Grindlay, J. E. 1986, *ApJ*, 308, 576
- Begelman, M. C., Blandford, R. D. & Rees, M. J. 1984, *Rev. Mod. Phys.* 56, 255
- Biretta, J. A. 1999, In *The Radio Galaxy M87*, Eds, H.-J. Röser and K. Meisenheimer, p 159 (Springer: Berlin)
- Biretta, J. A., Stern, C. P. & Harris, D. E. 1991, *AJ*, 101, 1632
- Biretta, J. A., Sparks, W. B. & Macchetto, F. D. 1999, *ApJ*, 520, 621
- Böhringer, H. et al. 2001, *A&A*, 365, L181
- Burbidge, G. R., Jones, T. W. & O’Dell, S. L. 1974, *ApJ*, 193, 43
- Burn, B. J. 1973, *MNRAS*, 165, 421
- Cavallo, G., Horstman, H. M. & Muracchini, A. 1980, *A&A*, 86, 36
- Dermer, C. D. 1995, *ApJ*, 446, L63
- Dermer, C. D., Sturmer, S. J. & Schlickeiser, R. 1997, *ApJS*, 109, 103
- Ginzburg, V. L. 1957, *Uspekhi Fiz. Nauk*, 62, 37
- Harris, D. E., Biretta, J. A. & Junor, W. 1997, *MNRAS*, 284, L21

- Harris, D. E., Biretta, J. A. & Junor, W. 1999, In *The Radio Galaxy M87*, Eds, H.-J. Röser and K. Meisenheimer, p 319 (Springer: Berlin)
- Jaffe, W. J. & Perola, G. C. 1973, *A&A*, 26, 421
- Junor, W. & Biretta, J. A. 1995, *AJ*, 109, 500
- Kardashev, N. S. 1962, *Sov. Astron - AJ*, 6, 317
- Keel, W. C. 1988, *ApJ*, 329, 532
- Kirk, J. G. 2001, In *Particles and Fields in Radio Galaxies*, ASP Conference Series, Eds. R. A. Laing & K. M. Blundell (Astronomical Society of the Pacific) (in press)
- Macchetto, F. D., Marconi, A., Axon, D. J., Capetti, A., Sparks, W. & Crane, P. 1997, *ApJ*, 489, 579
- Mannheim, K., Krülls, W. M. & Biermann, P. L. 1991, *A&A*, 251, 723
- Marscher, A. P., Marshall, F. E., Mushotzky, R. F., Dent, W. A., Balonek, T. J. & Hartman, M. F. 1979, *ApJ*, 233, 498
- Marscher, A. P. 1983, *ApJ*, 264, 296
- Meisenheimer, K., Röser, H.-J. & Schlötelburg, M. 1996, *A&A*, 307, 61
- Neumann, M., Meisenheimer, K., Röser, H.-J. & Fink, H. H. 1997, *A&A*, 318, 383
- Owen, F. N., Hardee, P. E., & Cornwell, T. J. 1989, *ApJ*, 340, 698
- Pérez-Fournon, I., Colina, L., González-Serrano, J. I. & Biermann, P. L. 1988, *ApJ*, 329, L81
- Perlman, E. S. Biretta, J. A., Sparks, W. B., Macchetto, F. D. & Leahy, J. P. 2001, *ApJ*, 551, 206
- Schreier, E. J., Gorenstein, P. & Feigelson, E. D. 1982, *ApJ*, 261, 42
- Stark, A. A., Gammie, C. F., Wilson, R. W., Bally, J., Linke, R. A., Heiles, C. & Hurwitz, M. 1992, *ApJS*, 79, 77
- Tonry, J. L. 1991, *ApJ*, 373, L1
- Tregillis, I. L., Jones, T. W. & Ryu, D. 2001, *ApJ*, 557, 475
- Whitmore, B. C., Sparks, W. B., Lucas, R. A., Macchetto, F. D. & Biretta, J. A. 1995, *ApJ*, 454, L73
- Wilson, A. S., Young, A. J. & Shopbell, P. L. 2001, *ApJ*, 547, 740

Table 1. Distances of jet knots from the nucleus (arc secs)

Waveband	D	E	F	A	B
X-ray	2.6	5.7 - 5.9	8.1	12.2 - 12.3	14.1
Optical	3.1	6.1	8.4 - 8.5	12.2 - 12.3	14.2
Radio	3.0 - 3.1	5.8 - 6.0	8.6 - 8.8	12.3 - 12.4	14.3 - 14.5

Table 2. Spectral fits to the X-ray emission of the nucleus and jet knots

(1) Name	(2) X <sup>a</sup> , Y <sup>a</sup> (arc sec)	(3) Region <sup>b</sup>	(4) N <sub>H</sub> <sup>c,d</sup> ( $\times 10^{20} \text{ cm}^{-2}$ )	(5) $\Gamma$ <sup>e</sup>	(6) K <sup>f</sup>	(7) $\chi^2$ (degrees of freedom)
Nuc (small) <sup>g</sup>	0, 0	1'' sqr	$6.1^{+1.5}_{-1.4}$	$2.17^{+0.10}_{-0.10}$	$23.1^{+1.8}_{-1.4}$	101.8 (106)
Nuc (large) <sup>g</sup>	0, 0	2''5 circ	$7.4^{+1.5}_{-1.4}$	$2.25^{+0.10}_{-0.09}$	$40.5^{+2.4}_{-2.9}$	145.2 (123)
D <sup>g</sup>	2.6, 1.0	1''5 circ	$0.90^{+2.0}_{-0.9}$	$2.04^{+0.16}_{-0.14}$	$8.41^{+0.72}_{-0.78}$	63.6 (60)
E	5.6, 2.1	1''5 circ	$3.8^{+3.4}_{-2.4}$	$2.32^{+0.26}_{-0.19}$	$2.34^{+0.50}_{-0.24}$	45.8 (39)
F	7.7, 2.9	1''5 circ	$5.6^{+2.4}_{-1.6}$	$2.90^{+0.44}_{-0.25}$	$1.96^{+0.31}_{-0.28}$	24.6 (32)
I	10.1, 3.8	1'' sqr	$4.2^{+7.0}_{-3.0}$	$2.49^{+0.50}_{-0.54}$	$0.81^{+0.24}_{-0.17}$	10.2 (13)
A <sup>g</sup>	11.6, 4.4	2''0 circ	$1.3^{+1.2}_{-1.1}$	$2.32^{+0.11}_{-0.10}$	$20.9^{+1.4}_{-1.1}$	152.4 (98)
B (small)	13.3, 5.1	1''5 circ	$2.1^{+3.0}_{-1.9}$	$2.28^{+0.24}_{-0.18}$	$2.10^{+0.38}_{-0.20}$	69.2 (39)
B (large)	13.3, 5.1	2''5 circ	$1.7^{+1.9}_{-1.6}$	$2.24^{+0.18}_{-0.09}$	$3.97^{+0.50}_{-0.29}$	72.0 (70)
C	16.3, 6.5	1''6 $\times$ 1''2 rect	$3.3^{+10.0}_{-3.3}$	$2.54^{+0.88}_{-0.51}$	$0.64^{+0.33}_{-0.10}$	14.3 (14)
C + G <sup>h</sup>	17.3, 7.0	3''4 $\times$ 2''0 rect	$4.3^{+4.3}_{-3.2}$	$2.07^{+0.30}_{-0.21}$	$2.36^{+0.70}_{-0.34}$	46.2 (46)

<sup>a</sup>Separation of center of region from the peak of the nuclear source in R.A. (X) and Dec (Y).

<sup>b</sup>Description of region from which spectrum was extracted. The diameter is given for circles and the side lengths for squares and rectangles.

<sup>c</sup>Equivalent hydrogen absorbing column.

<sup>d</sup>All errors are 90% confidence for a single parameter of interest.

<sup>e</sup>Photon index.

<sup>f</sup>Normalisation of power law model, in units of  $10^{-5} \text{ photons keV}^{-1} \text{ cm}^{-2} \text{ s}^{-1}$  at 1 keV.

<sup>g</sup>Spectra were obtained from 0.4 frame time observations.

<sup>h</sup>This region includes only part of the knot referred to as G in optical and radio observations.



Fig. 1.— Grey scale (upper panel) and contour (lower panel) representations of the X-ray emission of the M87 jet in the 0.1 - 10 keV band. For the upper panel, the image was rebinned to have a pixel size of 0.1 arcsec and then smoothed by a Gaussian with a FWHM = 0".5. This rebinning was not done for the contour map to retain the original number of counts pixel<sup>-1</sup>. The grey scale is proportional to the square root of the X-ray brightness, and ranges from 0.02 times the peak (white) to the peak (black). Contours are plotted at 20, 30, 60, 120, 180, 300, 400, 550, 700, 900 and 1000 counts pixel<sup>-1</sup>. The field plotted contains fainter, diffuse X-ray emission from M87 and the Virgo cluster; this emission is not shown in order to emphasise the jet.

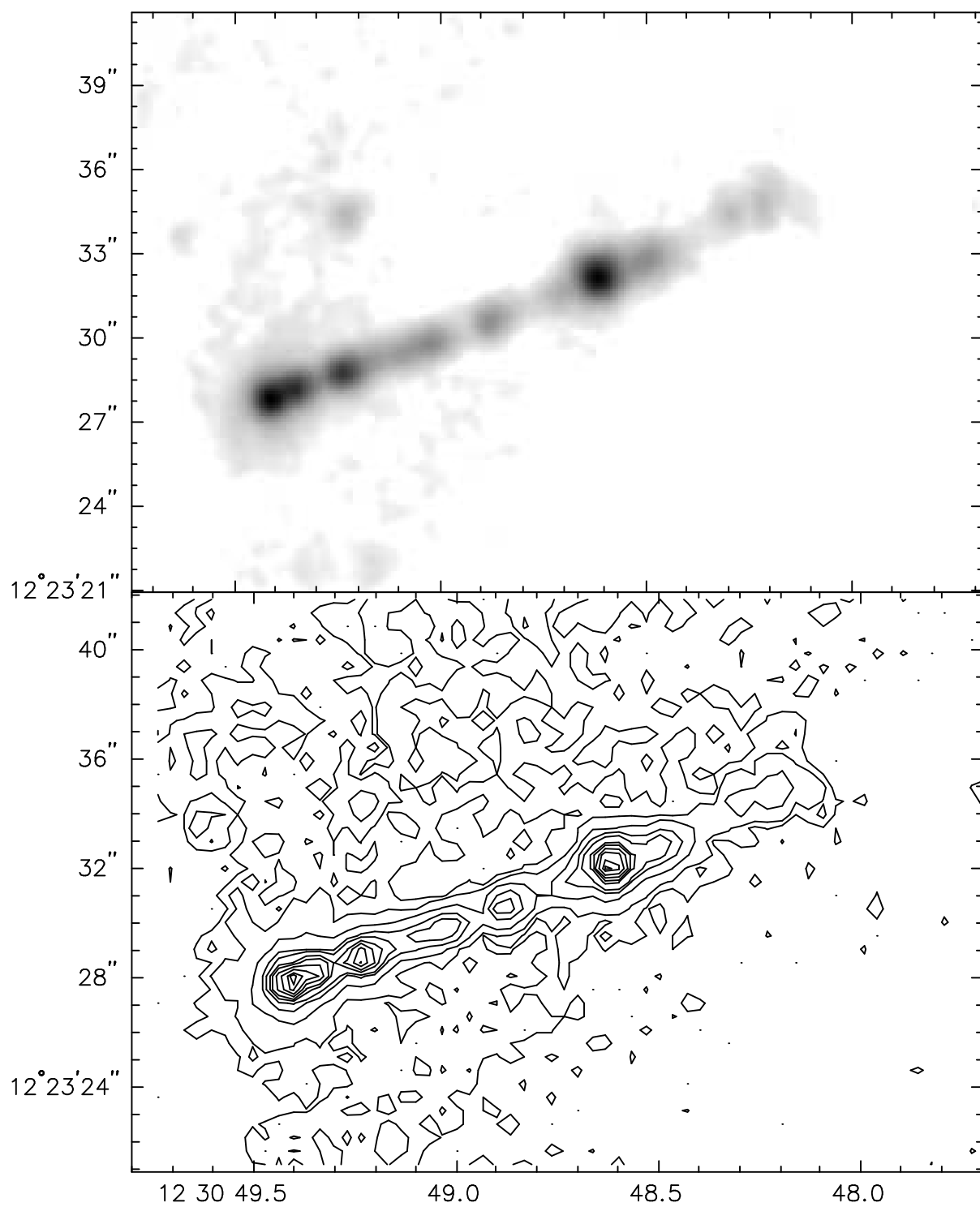
Fig. 2.— Grey scale representations of a 6 cm radio (top panel; Biretta, private communication), an optical V band (middle panel; Pérez-Fournon, private communication) and the Chandra X-ray (lower panel, 0.1 - 10 keV band) image. In the radio image, the grey scale is proportional to the square root of the brightness and ranges from 0.0003 (white) to 0.03 (black) Jy beam<sup>-1</sup>. In the optical image, the grey scale is also proportional to the square root of the brightness, ranging from 20 to 2016 counts pixel<sup>-1</sup>. The X-ray image is the same as in Fig. 1. The labels in the lower panel refer to the knots vertically above the label. N is the nucleus.

Fig. 3.— Plots of the brightness profiles along the M87 jet at 6 cm radio (solid line), V band optical (dotted line) and 0.1 - 10 keV X-rays (dashed line). Background emission from the surrounding diffuse X-ray emission has been subtracted from the X-ray profile. In producing these profiles, emission over a region 3" perpendicular to the jet axis was summed at each location at each wavelength. It is notable that the X-ray knots D and F, and possibly knot E, are displaced towards the nucleus from their radio and optical counterparts.

Fig. 4.— The radio through X-ray spectra of the various knots in the jet and the nucleus of M87. Filled squares are from Pérez-Fournon et al. (1988), asterisks are from Keel (1988), filled circles are from Biretta, Stern & Harris (1991) and filled triangles are from Perlman et al. (2001). The “bow tie” represents the X-ray spectrum, with its 90% confidence uncertainties, from our Chandra observations. The differences in the measured optical spectra of knots E and I may result from overestimation of the flux of these weak knots in ground-based observations (asterisks and circles). The X-ray spectrum given for knot G contains flux from the optical/radio locations of both knots C and G and does not represent the X-ray spectrum of knot G alone.

Fig. 5.— Plots of the optical to X-ray ( $\alpha_{\text{ox}}$ ), radio to X-ray ( $\alpha_{\text{rx}}$ ) and X-ray ( $\alpha_{\text{x}}$ ) spectral indices for the knots in the jet as a function of distance from the nucleus. The key is given in the upper left. Here optical means 6000 Å, radio 2 cm and X-ray 1 keV. The errors on

$\alpha_{\text{ox}}$  and  $\alpha_{\text{rx}}$  are smaller than the symbol sizes and are not shown. The error bars represent the 90% confidence errors on  $\alpha_{\text{x}}$ .



This figure "f2.jpg" is available in "jpg" format from:

<http://arxiv.org/ps/astro-ph/0112097v1>

